

## MASS LOSS IN ALPHA CYGNI: SYNTHETIC H-ALPHA PROFILES

PAUL B. KUNASZ  
 Boulder, Colorado

AND

NANCY D. MORRISON

Ritter Astrophysical Research Center, The University of Toledo

Received 1982 March 8; accepted 1982 June 2

### ABSTRACT

Observations by Inoue show that the H $\alpha$  profile in  $\alpha$  Cygni (A2 Ia) is characterized by shallow, shortward-shifted absorption, with an intensity longward of the rest wavelength that is at or above the continuum level. We interpret these characteristics in terms of a model stellar envelope that is spherically symmetric, expands with monotonically increasing velocity, and obeys mass flux continuity from the thermally controlled regime below the photosphere to the layers outside the line formation zone of H $\alpha$ . The principal free variables are the mass loss rate, the wind velocity law, and the Doppler broadening velocity law. The statistical equilibrium equations are solved for a six-level hydrogen atom in the comoving frame of the fluid, with the resonance transitions included explicitly, and with the intrinsic line profile assumed to be Gaussian. In the transformation to the observer's frame and calculation of the emergent flux profile in H $\alpha$ , the Gaussian is replaced by a Stark profile whose shape is a function of temperature, electron density, and the total Doppler broadening speed.

If the synthetic profiles are to match the observed profiles, the underlying photospheric absorption line must be filled in by emission, and the calculations show that the emission strength is very sensitive to the assumed mass loss rate. With the other free parameters fixed, the profile fitting determines  $\dot{M}$  to within about  $\pm 25\%$ . Both models with and models without supersonic Doppler broadening velocities can match the observed profile; the former models require a mass loss rate that is near  $\dot{M} = 1.7 \times 10^{-7} M_{\odot} \text{ yr}^{-1}$ , while the latter require  $\dot{M} = 4.0 \times 10^{-7} M_{\odot} \text{ yr}^{-1}$ . The range in all the free parameters that is allowed by observation suggests that the overall uncertainty in our derived mass loss rate is a factor of 2.

The computed line shape is sensitive to the velocity law assumed; various laws fit various individual profiles from Inoue's class *b* (those with smaller central intensity in the absorption feature). The present models cannot, however, match the shallower absorption features in class *a*.

*Subject headings:* line profiles — stars: individual — stars: mass loss

### I. INTRODUCTION

Alpha Cygni (A2 Ia) is the brightest and best-studied A type supergiant. Its position in the H-R diagram (Humphreys and Davidson 1979; see also § III) suggests that its main-sequence progenitor may have had a mass of 20–30  $M_{\odot}$  and a spectral type of O6–O9. Due to uncertainties in currently available evolutionary tracks for massive stars, however, these estimates are rough.

Lamers (1975) was the first to derive a mass loss rate for this star; he analyzed the Mg II resonance lines, which appear as shortward-shifted absorption features. The star is also known to show H $\alpha$  emission (e.g., Rosendhal 1972). This star's position in the H-R diagram makes determination of its mass loss rate extremely important, for two reasons. First, mass loss effects the evolutionary tracks of massive stars: in a major way for masses greater than 40–50  $M_{\odot}$ , and in at least a minor way for masses greater than about 15  $M_{\odot}$ . (For a review of this subject, see de Loore 1980; for recent work, see

Brunish and Truran 1981.) The exact magnitude of the effect of mass loss is unknown, however, since no generally accepted theoretical prescription exists for the scale of the mass loss rate or its dependence on stellar mass, luminosity, and temperature. On the other hand, observational progress in this direction is being made, both for O stars (Garmany *et al.* 1981) and for M supergiants (de Loore 1980). Since  $\alpha$  Cyg is intermediate in evolutionary phase between these two types of stars, determination of its mass loss rate will be crucial for the development of a coherent picture of mass loss as a function of position in the H-R diagram.

Second, the paucity of theoretical information on mass loss rates is partly due to the fact that the driving mechanism is still uncertain. While radiation pressure certainly plays a role, the importance of atmospheric motions in transmitting mechanical energy to the wind is unknown. Several authors have tested theoretical predictions against the empirical dependence of mass loss

rate on stellar luminosity and temperature for O and B stars (Lamers 1981; Garmany *et al.* 1981). Whether a well-determined mass loss rate for a significantly cooler star obeys the same law would be an important test of theories of stellar mass loss, provided the same driving mechanism operates.

Conti (1978) has reviewed the semiempirical determination of mass loss rates in O and B stars. The spectroscopic diagnostics he discusses have also been applied to  $\alpha$  Cyg. First are the ultraviolet resonance lines. In  $\alpha$  Cyg, only the singly ionized metals show shortward-shifted absorption features (but no P Cygni-type emission; see Praderie, Talavera, and Lamers 1980). There is no good evidence for such features in lines of neutral metals, while few resonance lines of doubly ionized metals are in the accessible ultraviolet. The best case is Al III  $\lambda\lambda$ 1854.7, 1862.8, which show neither shift nor asymmetry in our high-resolution *IUE* spectra of  $\alpha$  Cyg; see also Praderie, Talavera, and Lamers (1980).

The analysis of the Mg II resonance doublet  $\lambda\lambda$ 2795.5, 2802.7 by Kunasz and Praderie (1981) is the most recent and most thorough. They concluded, first, that the great breadth of the saturated absorption requires a micro-turbulent velocity that increases with height, reaching supersonic values in most of the extent of the wind. Second, the reason for the absence of P Cygni-type emission in the line is probably that photons removed from the shortward side of the line by scattering in an expanding wind are reemitted on the longward side, but only just fill in the longward damping wing of the photospheric line. Although their calculation did not include blending photospheric lines, such lines may also contribute to hiding the P Cygni emission. Third, the population of Mg<sup>+</sup> ions in the wind is determined by the stellar flux at the threshold wavelength for ionization of Mg<sup>+</sup> to Mg<sup>++</sup>; depending on the magnitude of this flux, successful models have  $\dot{M}$  ranging from  $3.1 \times 10^{-9}$  (which corresponds to dominance of the ionization balance by Mg<sup>+</sup>) to  $1.5 \times 10^{-7} M_{\odot} \text{ yr}^{-1}$ .

Hensberge *et al.* (1982) analyzed the shortward-shifted components of low-lying multiplets of Fe II in the wavelength range 2100–2800 Å. They found that blending photospheric absorption lines cancel the P Cygni-type emission produced in the wind. From the lack of a shortward-shifted component in the Al III resonance lines, they derive an upper limit to the population ratio of Fe<sup>++</sup> to Fe<sup>+</sup>, and conclude that  $\dot{M} < 5 \times 10^{-9} M_{\odot} \text{ yr}^{-1}$ .

Long-wavelength excess flux, interpreted as free-free emission from an extended ionized volume, has also been interpreted in terms of mass loss in  $\alpha$  Cyg. From an observation at 10  $\mu\text{m}$ , Barlow and Cohen (1977) derived  $\dot{M} = 6.9 \times 10^{-7} M_{\odot} \text{ yr}^{-1}$ . On the other hand, Abbott *et al.* (1980) failed to detect the star at 6 cm, and assigned an upper limit,  $\dot{M} < 2.5 \times 10^{-7} M_{\odot} \text{ yr}^{-1}$ . Subsequent attempts at detection suggest that this limit should be lowered to  $1.5 \times 10^{-7} M_{\odot} \text{ yr}^{-1}$  (Abbott 1980).

In the present work, we have performed semiempirical modeling of the H $\alpha$  profile in  $\alpha$  Cyg, with the aim of estimating the mass loss rate and further constraining the physical state of the stellar wind. As was done in

the analyses discussed above, we have assumed that spherical symmetry and mass flux continuity hold. Observations of time variability in the spectrum of  $\alpha$  Cyg, however, give grounds for questioning these assumptions. From an analysis of the radial velocities of visible-region absorption lines, Lucy (1976) found variation with a broad range of periodicities and concluded that the star's atmosphere undergoes many kinds of large-scale motion. If these motions are coupled to the wind, then the wind should also depart from spherical symmetry in a time-dependent way. Indeed, Inoue (1979) found time variability in the H $\alpha$  profile that encompasses a range of a factor of 2 in depth below the continuum at any given wavelength in the line. The general character of the line profile does not vary, however, and we expect the above structural assumptions to lead to a good estimate of the average mass loss rate.

Features of these calculations that are not often found in models of stellar winds are that the Sobolev approximation is not used and that thermal and micro-turbulent broadening are included self-consistently in the depth-dependent hydrogen absorption profile. In addition, the calculations account for the effect of the resonance lines on the populations of the upper levels by including the resonance lines explicitly and by treating a sufficiently large volume in the wind that Ly $\alpha$  is computed throughout most of its formation zone.

In the following, § II presents the observational material that we have fitted with these models. Section III presents the physical assumptions and parameterizations on which the models are based. Section IV presents the numerical methods, § V the results, and § VI our conclusions, along with a discussion of the validity of our assumptions and a comparison of our preferred value for the mass loss rate, which is near  $10^{-7} M_{\odot} \text{ yr}^{-1}$ , with previous determinations.

## II. OBSERVATIONAL MATERIAL

Figure 1 shows three typical profiles from the collection presented by Inoue (1979). For comparison, it also gives the theoretical profile calculated by Kurucz (1979) for a model atmosphere with  $T_{\text{eff}} = 9500$  K,  $\log g = 1.5$ , and solar abundances, which we find to be a nearly optimal choice (see § III). Although the three observed profiles show considerable variety, all show the general features our models must replicate, namely that the longward half of the line is filled in with emission, which sometimes extends above the continuum, and that the Stark-broadened photospheric profile forms a lower envelope to the shortward wing of the observed profile.

Inoue (1979) divided his spectroscopic results into two classes, which are defined by the radial velocities,  $v_R$ , of the lines Si II(2)  $\lambda\lambda$ 6347, 6371. In class *a*,  $+0.4 \leq v_R \leq +1.3$  km s<sup>-1</sup>. In the concurrent H $\alpha$  profiles, the normalized intensity at the absorption minimum,  $I_{\text{min}}$ , is between 0.7 and 0.8, except for one case in which  $I_{\text{min}} = 0.61$ . The long-dashed curve in Figure 1 is an example. This class of profile accompanies relatively small central

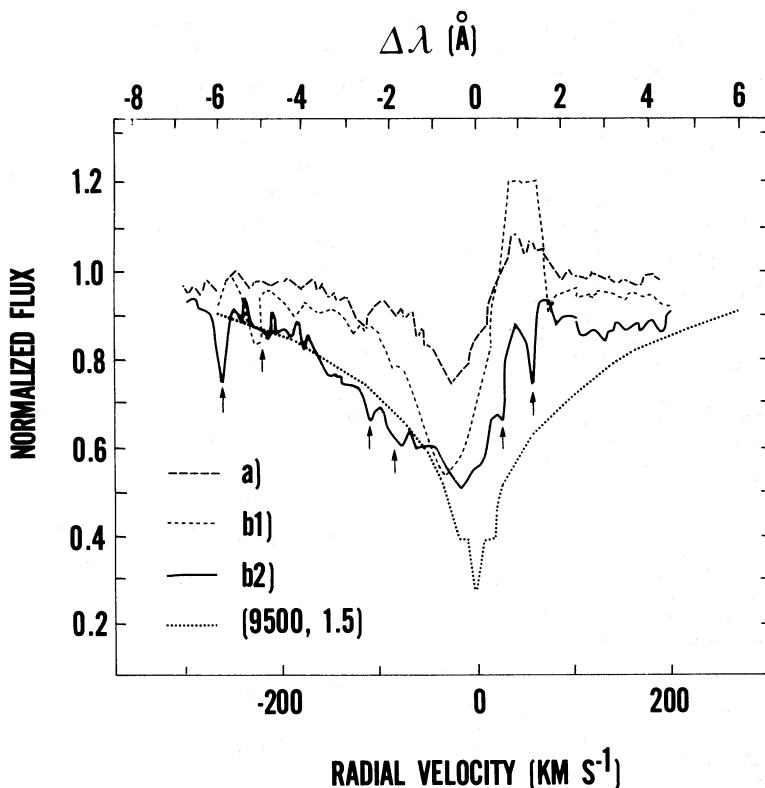


FIG. 1.—Comparison of observed  $H\alpha$  line profiles by Inoue (1979) with the photospheric profile predicted by a Kurucz (1979) model atmosphere with  $(T_{\text{eff}}, \log g) = (9500, 1.5)$  (dotted curve). The observed profiles consist of one example of class *a* (long dashed curve) and two examples from class *b* (short-dashed curve and solid curve; *b1* and *b2*). The vertical arrows indicate the positions of telluric water vapor lines.

depth in  $H\gamma$  and in strong lines of  $Mg\ II$ ,  $Si\ II$ , and  $Fe\ II$ . In class *a*, the intensity of the emission peak varies through a range of 10 or 12% of the continuum intensity. For the  $Si\ II$  lines in class *b*,  $-6.2 \leq v_R \leq -5.2\ \text{km s}^{-1}$ . The corresponding  $H\alpha$  profiles have  $0.4 \leq I_{\text{min}} \leq 0.5$ , and have a much larger range in emission strength. Examples are the short-dashed curve and the full curve in Figure 1. Class *b* spectra also include a relatively large central depth in  $H\gamma$  and the singly ionized metals. Variability in the observed flux at the emission peak is at least partly due to variability in the strength of a coincident telluric water vapor line. In all the  $H\alpha$  profiles, the absorption minimum occurs  $25\text{--}30\ \text{km s}^{-1}$  shortward of line center, and greater absorption width generally accompanies greater absorption depth.

### III. ATMOSPHERIC MODELS AND PARAMETERS

In our models, the layers are spherically symmetric, with the flow velocity everywhere satisfying mass flux continuity. For numerical convenience, we have divided the atmosphere into two parts separated by a transition layer. Below it are layers that are nearly hydrostatic and plane-parallel (the photosphere), and above it are spherically symmetric, accelerating layers (the wind). Although these regions are characterized by separate physics and separate parameterizations of the physical

variables, continuity across the boundaries is enforced for the wind speed  $v(r)$ , the microturbulent speed  $v_M(r)$ , the electron temperature  $T(r)$ , and the mass density  $\rho(r)$ .

The density and temperature as a function of height in the hydrostatic layers are given by a Kurucz (1979) model atmosphere with solar abundances. These models assume LTE and radiative equilibrium, and include line blanketing in the opacity. Our choice of  $T_{\text{eff}}$  and  $\log g$  stems from a fine analysis, based on Kurucz models, by Spessart and Morrison (1982). Using observations of the continuous energy distribution, the  $H\delta$  profile, and equivalent widths of  $Fe\ I$  and  $Fe\ II$  lines, they obtained  $T_{\text{eff}} = 9200 \pm 300\ \text{K}$  and  $\log g = 1.4 \pm 0.2$ . (A recent determination by Underhill 1981 yielded  $T_{\text{eff}} = 8600\ \text{K}$ , and a measurement of angular diameter by Bonneau *et al.* 1981 yielded  $8200 \pm 400\ \text{K}$ .) For convenience, we used the Kurucz model with  $T_{\text{eff}} = 9500\ \text{K}$  and  $\log g = 1.5$ .

The photospheric radius,  $R_{\text{ph}}$ , is also an important parameter, since, for a given mass loss rate, it controls the density throughout the wind. If the situation were optimal, we could assume the stellar radius to be known. In the present case, however, there is some uncertainty in the stellar luminosity. With  $T_{\text{eff}}$  fixed, the value of the radius depends on what luminosity is assumed. If, with Humphreys (1978), one assigns the star to membership in Cygnus OB7, then its absolute visual magnitude is

–8.4. With a bolometric correction of 0.2 mag, its luminosity is  $L = 2.2 \times 10^5 L_\odot$ . With  $T_{\text{eff}} = 9200$  K,  $R_{\text{ph}} = 190 R_\odot$ . There is reason, however, to doubt the star's membership in this association (Humphreys 1979). If it is a member, it is the most luminous A2 Ia supergiant in an association (Humphreys 1978; the next most luminous, HD 92693, has  $M_v = -8.1$ ). In addition, the  $B - V$  color excess of  $\alpha$  Cyg is substantially (about 0.6 mag) smaller than the average of the color excesses of the other luminous stars in Cyg OB7. If  $\alpha$  Cyg is not a member of Cyg OB7, then an estimate for its luminosity near the low end of the expected range is given by a low value among the other A2 Ia supergiants listed by Humphreys (1978), namely  $M_v = -6.7$ . With this value,  $L = 4.4 \times 10^4 L_\odot$  and, with  $T_{\text{eff}}$  as before,  $R_{\text{ph}} = 83 R_\odot$ . Bonneau *et al.* (1981) give  $R = 145 \pm 45 R_\odot$ , where most of the quoted uncertainty is due to the uncertainty in the stellar distance. While most of our models have  $R_{\text{ph}} = 150 R_\odot$ , we also constructed models with photospheric radii of 83 and 200  $R_\odot$ , with the results described in § V.

The basic structure of the wind is determined by the assumption that the density and the wind speed satisfy the equation of mass flux continuity,

$$\dot{M} = 4\pi r^2 \rho(r) v(r), \quad (1)$$

with the mass loss rate  $\dot{M}$  a constant and a free parameter. Then specifying  $v(r)$  determines  $\rho(r)$ , and the structure of the wind is given by  $v(r)$ ,  $v_D(r)$ , and  $T(r)$ , where  $v_D(r)$  is the total small-scale random velocity. We now discuss our assumptions about each of these variables in turn. In what follows,  $R_c$  and  $R_t$  ( $= 1.02R_{\text{ph}}$ ) denote the lower and the upper boundary, respectively, of the transition region, and their subscripts also label values of the other variables at these boundaries.

In the hydrostatic layers,  $\rho(r)$  is taken from a Kurucz (1979) model and  $v(r)$ , though minuscule, is defined from  $\rho(r)$  via equation (1). In the transition region between the hydrostatic and dynamic regions,  $v(r)$  is the linear function

$$v(r) = v_c + (v_t - v_c)(r - R_c)/(R_t - R_c), \quad (2)$$

where  $v_t = 10 \text{ km s}^{-1}$  and  $R_c \leq r \leq R_t$ . The transition region is not important in the computed profiles and serves merely as a smooth connection between the outermost zone of the hydrostatic region and the inner boundary of the dynamic region. For this reason, it is not detailed in Figure 2 (see below).

In the dynamic region ( $r > R_t$ ) we assume in all but one model,

$$v(r) = v_0 + (v_\infty - v_0)(1 - R_{\text{ph}}/r)^\beta. \quad (3)$$

In this law,  $v$  increases monotonically from  $r = R_t$ , approaching  $v_\infty$  as  $r \rightarrow \infty$ . The extension parameter,  $\beta$ , assumes values from 0.35 to 3.5, and  $v_0$  is chosen so that  $v_t \equiv v(R_t) = 10 \text{ km s}^{-1}$ . Since  $r = R_{\text{ph}}$  is in the static domain, flow with  $v = v_0$  never appears in the model. We emphasize that law (3) is employed only for  $r > R_t$ . It is the same as a family of laws often assumed for models

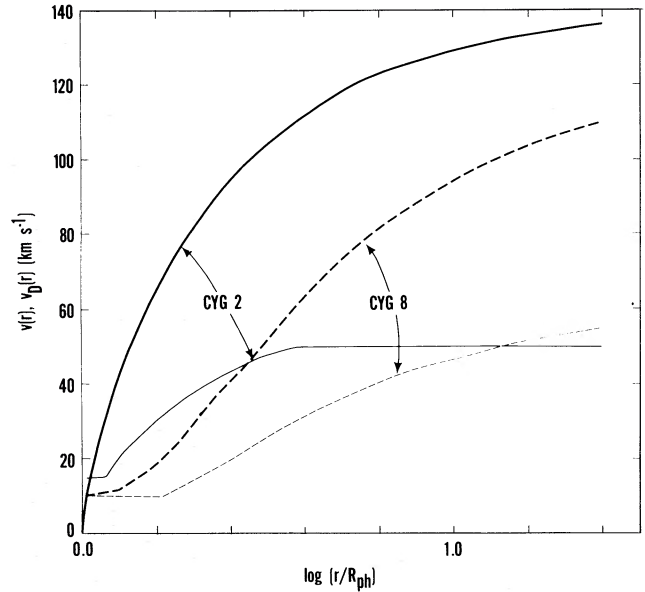


FIG. 2.—Wind speed and Doppler broadening speed as a function of radial distance (in units of the photospheric radius  $R_{\text{ph}}$ ) for two successful models: CYG 2: Heavy solid line,  $v(r)$ ; light solid line,  $v_D(r)$ . CYG 8: Heavy dashed line,  $v(r)$ ; light dashed line  $v_D(r)$ .

treated in the Sobolev approximation, except that the curve  $v(r)$  is vertically displaced so that  $v = 10 \text{ km s}^{-1}$  at  $r = R_t$ .

The value of  $R_c$  and the corresponding value of  $\tau_{500}$  in the model for the static layers are determined by the condition that density and column density be continuous at  $R_c$ , so that the total column density at  $R_{\text{ph}}$  will agree with that of the Kurucz model, and the upper layers will be smoothly mated to the static model. The wind speed at this height is given by the assumed mass loss rate  $\dot{M}$ , the value of  $R_c$ , and the density  $\rho_c$ , together with equation (1). For the values of  $\dot{M}$  and the functions  $v(r)$  chosen in the models, the interface  $R_c$  occurs at a density such that  $v(r_c) \ll (2kT/m_H)^{1/2}$  and  $\tau_{500} \sim 3 \times 10^{-3}$ . Table 1 summarizes  $v(r)$  and  $T(r)$  in the various regions of the models.

Our one model in which  $v(r)$  is not monotonically increasing incorporates the law (3) in the inner layers of the wind and ballistic deceleration in the outer layers. This model is unsuccessful in fitting the observed H $\alpha$  profile, in that it produces an additional minimum at about  $-150 \text{ km s}^{-1}$  in the absorption feature. Therefore, we will discuss it no further.

The variable  $v_D(r)$  includes both thermal and micro-turbulent speed, being defined by

$$v_D^2(r) = v_M^2(r) + 2kT(r)/m_H. \quad (4)$$

Our choice of  $v_D(r)$  and of the terminal wind speed,  $v_\infty$ , are based on the conclusions that Kunasz and Praderie (1981) reached from their analysis of the Mg II resonance lines. Our models are of two kinds. In the "nonturbulent" models,  $v_D = 10 \text{ km s}^{-1}$  throughout the wind and

TABLE 1  
SUMMARY OF TEMPERATURE AND VELOCITY LAWS

$r$	$v(r)$	$T(r)$
$< R_c$ .....	$\dot{M}/4\pi r^2 \rho(r)^a$	$T(\tau_{500})$ from Kurucz 1979: (9500, 1.5, 0.0)
$R_c$ .....	$\dot{M}/4\pi R_c^2 \rho_c; \ll (2kT/m_H)^{1/2}$	$T(\tau_c)$ from above
$R_c < r < R_t$ .....	$v_c + (v_c - v_t)(r - R_c)/(R_t - R_c)$	$T_{\text{eff}}(a\tau_{500} + b)^{1/4}$
$R_t (= 1.02R_{\text{ph}})$ .....	$v_t = 10 \text{ km s}^{-1}$	$T_{\text{eff}}(a\tau_{500} + b)^{1/4}$
$> R_t$ .....	$v_0 + (v_\infty - v_0)(1 - R_{\text{ph}}/r)^b$	$T_{\text{eff}}(a\tau_{500} + b)^{1/4}$

<sup>a</sup> A nonzero velocity in the "static" layers was used for strict consistency with mass flux continuity, even though zero velocity would produce essentially the same results.

$v_\infty = 260 \text{ km s}^{-1}$ , the value given directly by the wavelengths of the shortward edges of the Mg II lines. Kunasz and Praderie (1981) were, however, unable to reproduce the great breadth of saturation of the Mg II lines without assuming that  $v_M$  increases with height to a supersonic value. In our "turbulent" models, we choose  $v_M$  to be in the range that gives a correct velocity for the shortward edge of the Mg II resonance lines when the maximum wind speed is taken to be  $120 \text{ km s}^{-1}$ . Note that, since our approach requires spherical symmetry, it cannot treat macroturbulence in more than one dimension, and we did not attempt to model time-dependent features.

The radial variation of the temperature in the wind is assumed to be given in terms of  $T(\tau_{500})$  by the following variant of the gray law:

$$T(\tau_{500}) = T_{\text{eff}}(a\tau_{500} + b)^{1/4}, \quad (5)$$

where  $\tau_{500}$  is the continuous optical depth at 500 nm. The coefficients  $a$  and  $b$  are determined by the boundary conditions. The lower boundary condition is that  $T_c = T(\tau_c)$  be the temperature of the photospheric model atmosphere at a height corresponding to  $R_c$ , and the upper boundary condition is that  $T(\tau_{500} = 0) = T_0$ , a free parameter referred to as the asymptotic wind temperature. In terms of the radial coordinate,  $\tau_{500} = 0$  corresponds to  $r = R_{\text{max}}$ , the radius of the outermost shell in the numerical calculation.

The chemical constituents of the atmosphere are hydrogen, helium, and the most abundant light metals. In the determination of continuous opacities and emissivities, populations for the atomic states of helium, the metals, and their ions are calculated in LTE. Electron scattering and free-free electron absorption and emission are also accounted for. The treatment of background sources and sinks of radiation is exactly as described by Mihalas, Kunasz, and Hummer (1975). The model atom for hydrogen has six bound levels, with all bound-bound transitions treated on the same basis, plus transitions connecting the bound levels to the continuum.

#### IV. METHOD OF SOLUTION

Before describing our procedures in detail, we note that the physical situation we are modeling is more complex than is usual in stellar winds in hot stars. The reason is that, in our case, the three line-broadening speeds that characterize the problem—the Stark line

width (expressed in velocity units), the terminal wind speed, and the microturbulent speed—can be within a factor of 2 of each other. Therefore, the Sobolev approximation (Mihalas 1978, p. 471) is not suitable. In addition, it is essential to include the photospheric profile correctly; since this profile is broad and is only partly filled in by emission, its effect on the emergent line profile is large. Therefore, the equation of radiative transfer is solved from  $\tau_{500} \approx 30$  out to the asymptotic zone of the wind. In this way the underlying profile is included self-consistently, rather than introduced as a lower boundary condition (see, e.g., Hamann 1981; Olson and Ebbets 1981). Finally, in previous calculations, the wind was known in advance to be ionized. In the present case, however, the temperature in the wind may drop below 6000 K and the ionization balance may shift to H. Accordingly, our technique (see below) for computing the level populations of H treats the density of  $\text{H}^+$  consistently with the bound-state densities.

Our calculation proceeds in two principal stages: first, solution of the non-LTE statistical equilibrium equations for hydrogen in the comoving frame of the fluid; second, transformation to the observer's frame for the calculation of the emergent intensity and the emergent flux profile. To begin, the non-LTE statistical equilibrium calculation requires estimates of level populations for H, He, the most abundant light metals, and their ions. We obtain these estimates by solving the LTE equation of state on a mesh of radial coordinate values that smoothly samples the physical variables from  $\tau_{500} \sim 30$  to an outermost shell lying well outside the line formation zone of the subordinate transitions considered in a six-level model hydrogen atom.

From these starting populations, we obtain non-LTE level populations for H using the technique described by Mihalas and Kunasz (1978). It employs the equivalent-two-level-atom (ETLA) iteration scheme, which solves the individual line transfer equations in the comoving frame of the flow for six bound levels and the continuum.

In this phase of the calculation, the absorption profile of each transition in the fluid frame is assumed to be a Gaussian:

$$\phi(v, r) = \frac{1}{(\pi)^{1/2}} \frac{1}{\Delta v_D} \exp \left[ - \left( \frac{v - v_0}{\Delta v_D} \right)^2 \right], \quad (6)$$

with Doppler width  $\Delta v_D$  produced by the combined thermal and microturbulent frequency shifts,  $\Delta v_D(r) = (v_0/c)v_D(r)$ , where  $v_D(r)$  is defined by equation (4). For a large range of variation of  $\Delta v_D(r)$ , a set of frequency points,  $\nu_i$ , must be chosen to sample the profile accurately in all parts of the atmosphere. As in any scheme in which the equations are solved for linear corrections sequentially rather than simultaneously, convergence is not ensured. Nevertheless, all models treated here converged satisfactorily.

After obtaining converged non-LTE level populations, we calculate the frequency-integrated opacity and emissivity for any line of interest (e.g., H $\alpha$ ) in the hydrogen transition network. Together with the LTE background opacities and emissivities, they serve as input to the formal calculation of the emergent radiation field in the reference frame of a distant observer stationary with respect to the center of mass of the star.

While experience shows that the Gaussian approximation to the line profile is satisfactory in the comoving frame stage of the calculation, one must treat the details of line absorption and emission accurately when calculating the flux profile in the observer's frame. We incorporate the Stark profile for the lines of the Balmer series using the approximation of Griem (1964), which, for typical photospheric temperatures and densities, deviates from the more accurate results of Vidal, Cooper, and Smith (1973) by less than 10%. In the wing, where the error maximizes, we incorporate a correction for it. Our numerical techniques include the dependence of this profile on depth, both through the sensitivity of the Stark wing to density, and through the large variation of the Doppler width.

We needed to generalize the observer's frame calculation as presented by Mihalas and Kunasz (1978), for the following reason. In their treatment, the line profile function reaches one maximum for any one frequency within the line, along any chosen line of sight (hereafter, "ray"). (See Mihalas and Kunasz 1978, p. 646.) In our case, the profile function depends not only on  $v_D$ , and the component of the wind velocity along the ray, but also on temperature and electron density. For observer's frequencies in the shortward wing of the Stark profile and for rays striking the stellar photosphere, the profile function may have two relative maxima. The outer maximum is a resonance, which occurs where the wind velocity vector projected along the line of sight produces a Doppler shift of the emitted frequency to match the observer's frequency, as in the work just cited. In a wind with  $d|v|/dr > 0$ , only one such resonance may occur. The second maximum occurs in the static layers, where the profile function is evaluated at the observer's frequency but the wing value is greatly elevated by the high electron density. The large value of the line source function in the static layers may more than compensate for the fact that the profile is evaluated in the wing and that these layers are partially obscured by the outer zone where resonance occurs. Therefore, we generalized the observer's frame calculation to sample completely all relevant zones along each ray. This generalization also allows the treatment, in the observer's

frame calculation only, of decelerating or of infalling flows.

In the statistical equilibrium step of the overall calculation, the inclusion of resonance lines in the transition network presents obstacles which, for some models, can be great or insurmountable. The fact that the line opacity of Ly $\alpha$  can be more than 10 orders of magnitude greater than that of H $\alpha$  severely constrains the radial grid spacing and requires inclusion of an enormous volume outside the line formation zone (LFZ) of the subordinate lines to encompass the LFZ of Ly $\alpha$ . Since H $\alpha$  and the other subordinate lines are thin in most of the LFZ of Ly $\alpha$ , and Ly $\alpha$  is extremely thick in the LFZ of H $\alpha$ , the temptation is to confine the explicitly treated transition network to the subordinate lines, and to treat the resonance line rates in radiative detailed balance or some other approximation for saturated lines. Though most treatments of H $\alpha$  in the literature assume the resonance lines to be in detailed balance, caution is necessary in the case of a stellar wind with low density and high velocity gradient. In all models considered here, the resonance lines are treated explicitly, with the qualification that, far outside the line formation zone of H $\alpha$ , density is allowed to fall off more rapidly than  $1/r^2$  to avoid extremely large values of  $R_{\max}$ , which are costly to treat. We did construct one model (CYG 19) with  $R_{\max} = 100R_{\text{ph}}$ , which confirmed that the smaller values of  $R_{\max}$  used in the other models result in adequate treatment of the resonance lines. This model also served to check the ionization state of hydrogen in the outermost layers (see § VI).

As a general rule, models with a wind sufficiently dense to fill in a large fraction of the H $\alpha$  photospheric absorption line converged rapidly to level populations largely independent of the resonance rates. On the other hand, in less dense winds, convergence required as many as 30 ELTA iterations, and the inclusion of the resonance rates increased the converged populations of the excited states. Models in the former category were usually iterated to convergence with the resonance lines in detailed balance, then iterated twice more with the resonance lines included. If the final two iterations produced only minor changes in the populations of the LFZ of H $\alpha$ , no further iterations were done.

Convergence was also aided by inclusion of a cycle of  $\Lambda$ -iterations after each cycle through the non-LTE line calculations. In a  $\Lambda$ -iteration, the radiation field is recalculated on the basis of the current population estimates. The effect is to allow the radiation field, and therefore the radiative rates, to relax to values determined by the current populations.

The frequency quadratures in the comoving frame and observer's frame were defined conservatively and tested for accuracy. The observer's frame calculation of the detailed radiation field was carried out on 49 observer's frequency values, in order to sample thoroughly the emergent flux profile, and the flux angle quadrature was carried out on a set of at least 80 rays. At each frequency, on each ray, the formal calculation of emergent intensity is carried out on the intersection of the ray with the original radial mesh ( $\geq 70$  radii), refined

to include all points along the ray at which the frequency argument of the observer's absorption profile passes through 80 preassigned values. These frequencies were carefully chosen for accurate sampling of the absorption profile in both the dense lower layers, where the photospheric line wings are formed, and the accelerating or rapidly moving outer layers. Of course, not all frequency-ray combinations intersect all 80 co-moving frequency argument values; and, if the original radial mesh is extremely dense in some interval of radius, the set of rays need not be one-to-one with the set of radii.

### V. RESULTS

Of the 60 models we investigated, the most successful are listed in Table 2, which gives the free parameters, together with a characteristic of the velocity law. The only parameter not listed is  $T_0$ , which is 6000 K unless otherwise specified. The left-hand column gives the name of the model. The remaining columns list: (1) the photospheric radius,  $R_{ph}$ , in units of the solar radius; (2) the mass loss rate; (3) the exponent  $\beta$  in the velocity law (2); (4) the terminal velocity  $v_\infty$ , in  $\text{km s}^{-1}$ ; (5) the value of  $r$ , in units of  $R_{ph}$ , at which  $v(r) = 50 \text{ km s}^{-1}$ , a radial velocity that is important in the line profile; (6) the radius  $R_{max}$  of the outermost shell in the radial mesh, in units of  $R_{ph}$ ; (7) a summary of  $v_D(r)$  (explanation follows); and (8) comments giving any special characteristics of the model.

Two notations are used in column (7). The notation  $(a, b)(c, d)$  means that  $v_D$  increases from  $a$  to  $b$  linearly with  $v$  as  $v$  goes from  $c$  to  $d$ , i.e.,

$$v_D = a + (v - c)(b - a)/(d - c). \quad (7)$$

For  $v > d$ ,  $v_D = b$ .  $\text{MAX}(10, v/2)$  means that  $v_D = 10 \text{ km s}^{-1}$  or  $v/2$ , whichever is greater.

Figures 3–6 compare some of the synthetic profiles to each other and to line profiles belonging to Inoue's (1979) class *b*. We first attempted to fit the total emission strength or amount of filling in of the photospheric profile due to the overlying layers, which is very sensitive to electron density and hence to the assumed mass-loss rate. Figure 3 compares three profiles from models that are identical except for mass loss rate: CYG 13, 16, and 14, which have  $\dot{M} = (0.8, 4.0, \text{ and } 8.0) \times 10^{-7} M_\odot \text{ yr}^{-1}$ , respectively. An increase of only a factor of 2 in the mass loss rate transforms marginal emission (CYG 16) into a strong P Cygni-type profile (CYG 14). Thus, in principle, the emission strength determines  $\dot{M}$  tightly. Given the values of the free parameters assumed for this set of models, the observed profile requires  $\dot{M} = (4.0 \pm 1.0) \times 10^{-7} M_\odot \text{ yr}^{-1}$ . This error estimate is based on the change in  $\dot{M}$  that would be needed to produce a noticeably different synthetic profile, which we infer from the differences between profiles calculated from CYG 2, 3, and 4 (see Fig. 4).

In order to make an error estimate for  $\dot{M}$  that takes into account the allowable ranges in the free parameters, we examine models calculated for other choices of free parameters, in which compensating changes in  $\dot{M}$  again produce a good fit to the observed profile. The profiles in Figure 3 were computed from nonturbulent models, in which  $v_D = 10 \text{ km s}^{-1}$  throughout the wind and  $v_\infty = 260 \text{ km s}^{-1}$ . "Turbulent" models, in which  $v_D$  increases with radial distance to supersonic values and  $v_\infty = 120$  or  $140 \text{ km s}^{-1}$ , can match the observed profile equally well. Since Kunasz and Praderie (1981) found

TABLE 2  
MODELS AND MODEL PARAMETERS

Model	$R_{ph}/R_\odot$ (1)	$\dot{M}$ ( $M_\odot \text{ yr}^{-1}$ ) (2)	$\beta$ (3)	$v_\infty$ ( $\text{km s}^{-1}$ ) (4)	$R_{50}/R_{ph}$ (5)	$R_{max}/R_{ph}$ (6)	$v_D(r)$ (7)	Comments (8)
CYG 1	150	1.0 (-7)	1.00	140	1.5	20	(15, 50)(30, 110)	
2	150	2.0 (-7)	0.80	140	1.4	20	(15, 50)(30, 110)	
3	150	3.0 (-7)	0.80	140	1.4	20	(15, 50)(30, 110)	
4	150	4.0 (-7)	0.80	140	1.4	20	(15, 50)(30, 110)	
5	150	3.0 (-7)	0.35	140	1.2	20	(15, 50)(30, 110)	
6	150	3.0 (-7)	0.35	140	1.2	20	(15, 30)(10, 70)	
7	150	1.5 (-7)	2.50	120	2.0	20	MAX (10, $v/2$ )	
8	150	2.0 (-7)	2.50	120	3.0	40	MAX (10, $v/2$ )	
9	150	2.0 (-7)	2.50	120	3.0	40	MAX (10, $v/2$ )	Weak chromosphere
10	150	2.0 (-7)	3.50	120	3.9	40	MAX (10, $v/2$ )	
11	150	1.5 (-7)	2.50	120	3.0	40	MAX (10, $v/2$ )	For $6 \times 10^{-3} \leq \tau_{656} \leq 6 \times 10^{-2}$ , $T$ reduced below standard law <sup>a</sup>
12	83	6.0 (-8)	2.50	120	3.0	40	MAX (10, $v/2$ )	
13	150	8.0 (-8)	2.50	260	1.9	40	10	
14	150	8.0 (-7)	2.50	260	1.9	40	10	
15	150	1.5 (-7)	2.50	120	3.0	40	MAX (30, $v/2$ )	
16	150	4.0 (-7)	2.50	260	1.9	40	10	
17	150	1.5 (-7)	2.50	120	3.0	40	MAX (10, $v/2$ )	Steep $T$ rise to 11,000 K at $v_\infty/2$ ; then $T \rightarrow 12,000 \text{ K}$ as $r \rightarrow \infty$
18	200	8.0 (-7)	1.40	260	1.4	10	10	
19	150	1.7 (-7)	2.40	120	3.0	100	MAX (10, $v/2$ )	Resonance lines iterated to convergence outside LFZ of $\text{H}\alpha$

<sup>a</sup>  $\tau_{656}$  is continuous optical depth at  $\lambda = 6563 \text{ \AA}$ .

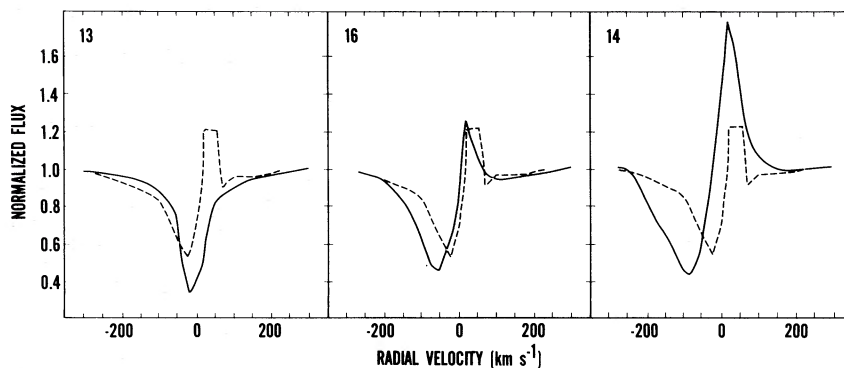


FIG. 3.—Comparison of the observed H $\alpha$  profile that we designate *b1* (dashed curves; see Fig. 1) with the synthetic profiles from models CYG 13, 16, and 14, which have mass loss rates of  $(0.8, 4.0, \text{ and } 8.0) \times 10^{-7} M_{\odot} \text{ yr}^{-1}$ , respectively. This comparison shows the great sensitivity of H $\alpha$  emission strength to the assumed mass loss rate.

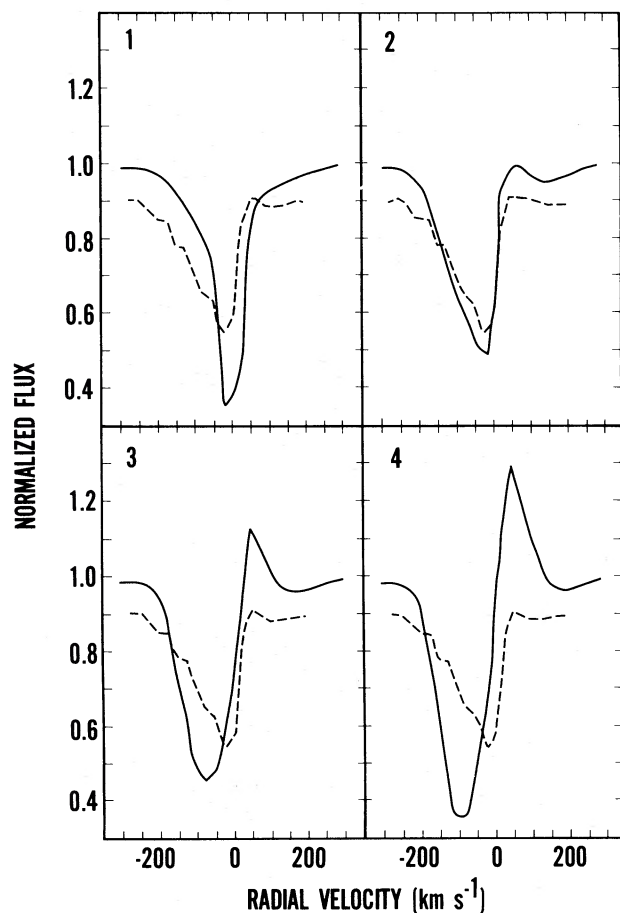


FIG. 4.—Comparison of the observed H $\alpha$  profile that we designate *b2* (dashed curves; see Fig. 1) with the synthetic profiles from models CYG 1, 2, 3, and 4, which have  $\dot{M} = (1.0, 2.0, 3.0, \text{ and } 4.0) \times 10^{-7} M_{\odot} \text{ yr}^{-1}$ , respectively (full curves). This comparison shows how the synthetic profile reacts to small changes in  $\dot{M}$  when the other parameters are held essentially fixed. It also shows that the synthetic profile from CYG 2 matches profile *b2* reasonably well, though it is a poor fit to *b1* (see Fig. 5).

that a highly supersonic turbulent velocity is required to match the widths of the Mg II resonance lines, the turbulent models are to be preferred. Although the values of  $v_D$  required are rather large, Hamann (1981) suggests that even larger values are required to match P Cygni profiles in O stars. Figure 4 shows profiles calculated from models CYG 1, 2, 3, and 4, each compared with the same observed profile. In each,  $v_D$  increases with height from 10 to 50 km s $^{-1}$ . All have nearly identical parameter sets except for the mass loss rates, which are  $(1.0, 2.0, 3.0, \text{ and } 4.0) \times 10^{-7} M_{\odot} \text{ yr}^{-1}$ , respectively. Model CYG 2 gives a good match to several profiles without emission above the continuum, but does not reproduce the narrower absorption feature of profile *b1* (see Fig. 5). Here, we estimate that an optimal match to profile *b2* would be given, for this parameter set, by  $\dot{M} = (1.7 \pm 0.4) \times 10^{-7} M_{\odot} \text{ yr}^{-1}$ . The reason that a smaller mass loss rate is required in this case is that an absorption profile greatly broadened by microturbulence in the wind traps more radiation than a less broadened

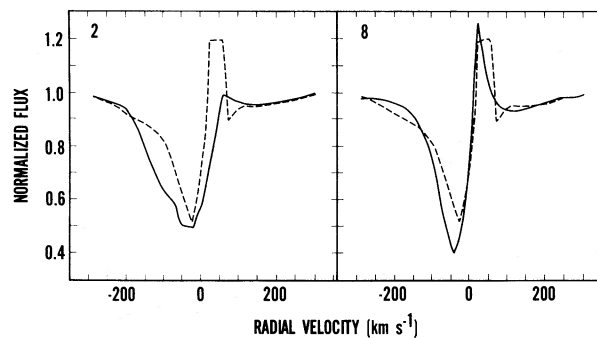


FIG. 5.—Comparison of the observed H $\alpha$  profile that we designate *b1* (dashed curves; see Fig. 1) with the synthetic profiles from models CYG 2 and CYG 8, which are essentially identical except that the values of  $\beta$  are 0.8 and 2.5, respectively (full curves). In CYG 2, note the greater absorption width and the near lack of emission above the continuum; this synthetic profile is a good match to observed profile *b2* (see Fig. 4).

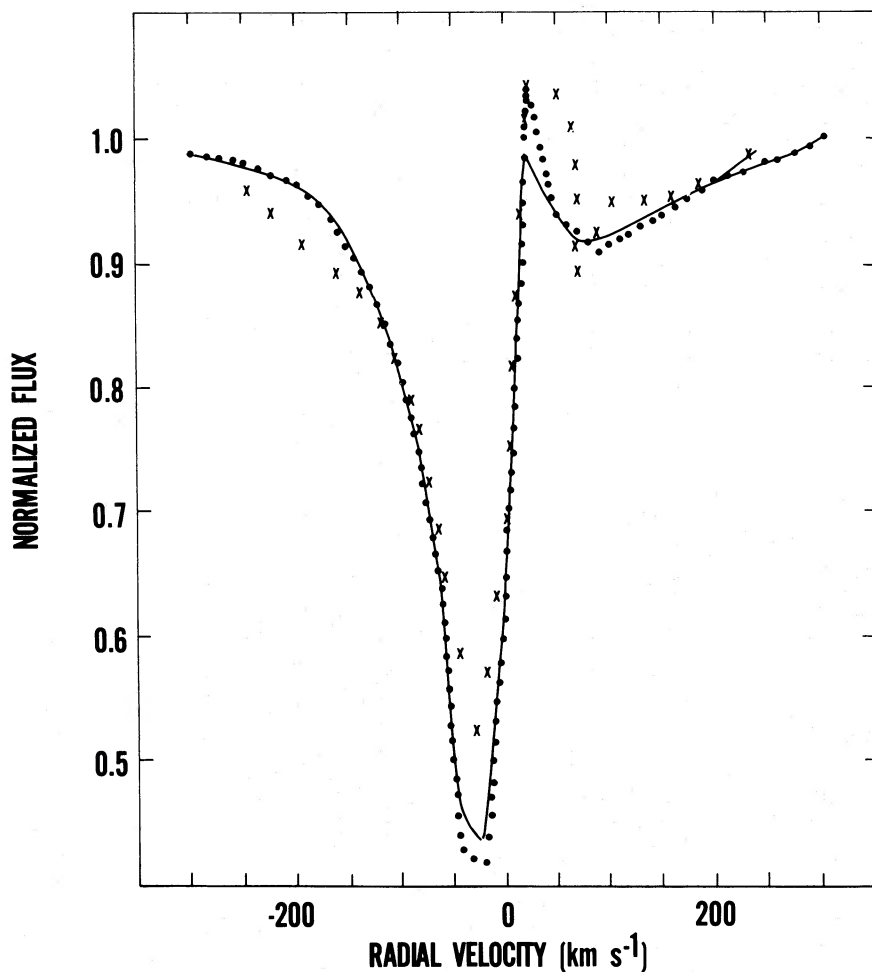


FIG. 6.—Comparison of the observed H $\alpha$  profile that we designate *b1* (crosses; see Fig. 1) with the synthetic profiles from model CYG 7 (full curve) and CYG 17 (dotted curve), which are identical except that CYG 17 includes a steep temperature rise (see Table 2). The comparison shows that the temperature rise makes almost no difference to the computed profile.

profile. The line source function is thereby increased in the highly broadened case, and both emission and violet-shifted absorption are enhanced for a given electron density.

Another degree of freedom comes from the fact that the observational uncertainty in the stellar luminosity allows a range in the photospheric radius. So far, we have been discussing models with  $R_{\text{ph}} = 150 R_{\odot}$ . For  $R_{\text{ph}} = 83 R_{\odot}$ , near the lower end of the acceptable range (see § III), a good match to the observed profile ensues if  $\dot{M} = (7.0 \pm 1.0) \times 10^{-8} M_{\odot} \text{ yr}^{-1}$ . In this case, the reason that a smaller mass loss rate provides a good fit is that the line profile is sensitive primarily to the electron density. If  $R_{\text{ph}}$  is reduced while  $n_e(r/R_{\text{ph}})$  is fixed, the total mass in the wind is smaller.

Having found several models that reproduce the observed emission strength, we attempted to fit the observed width, depth, and velocity of minimum intensity of the absorption feature. For mass loss rates giving the correct emission strength, these properties are

controlled by the degree of extension of the atmosphere, that is, the parameter  $\beta$  in the velocity law. In order to show the effect of varying  $\beta$ , Figure 5 compares synthetic profiles from CYG 2 and CYG 8, which have  $\beta = 0.8$  and 2.5, respectively. The other free parameters are similar in both; in particular, both have  $\dot{M} = 2.0 \times 10^{-7} M_{\odot} \text{ yr}^{-1}$ . CYG 10 (not plotted) is identical to CYG 8 except that  $\beta = 3.5$ . Its profile is similar to that from CYG 8, but with a narrower absorption feature. In general, larger values of  $\beta$  give a narrower absorption profile, but some observed profiles are narrower than any we were able to synthesize. Although model CYG 2 is an exception (Fig. 5), most models with  $\beta < 2$  give absorption minima at too short a wavelength.

In attempting to match the depth of the absorption feature, we encountered difficulty. Even the most successful profiles are slightly deeper than a typical class *b* profile with emission, and none successfully matches class *a* profiles. None of the following modifications was successful in reducing the depth of the synthetic profile

enough to fit class *a*. (i) Ballistically decelerating outer layers were placed above accelerating inner layers; Table 1 does not include these models. (ii) A large microturbulent speed in the static layers (CYG 15) produced a profile that is grossly too deep: it has  $I_{\min} = 0.30$  and no filling in by emission. (iii) Alterations in the temperature structure in the static layers were not successful and also are not included in Table 1. In any case, it is unlikely that the photospheric structure departs greatly from that of the Kurucz (1979) model atmosphere we chose, because Spessart and Morrison (1982) found that this model gives a good fit to all visible-light observations of the photosphere. Therefore, whatever mechanism fills in the central part of the absorption beyond the capability of our models to reproduce it probably operates above the line formation zone of  $H\delta$ . We recall, however, that Inoue and Uesugi's (1977)  $H\gamma$  central intensities are slightly larger for class *a* observations. Therefore, the filling-in mechanism may operate in layers at and above the place of formation of the core of  $H\gamma$ . (iv) An elevated temperature in the wind ("chromosphere") also does not increase the central intensity. Model CYG 9 includes a mild chromosphere, and model CYG 17 includes a stronger one, with  $T_0 = 12,000$  K. Figure 6 compares this model to CYG 7, which is identical except for including no temperature rise, and shows the computed

profiles to be nearly identical. We did not attempt a value of  $T_0$  higher than 12,000 K, because Praderie (1979) gave this value as an upper limit to the temperature of any substantial part of the wind, based on a search of the ultraviolet spectrum for chromospheric indicators.

Although we have discussed only  $H\alpha$  and  $H\delta$ , our results could also be used to calculate the profile of any other line in the network of transitions that we included explicitly. The reason is that the multilevel coupling in hydrogen demands that all the level populations in the network be converged in order for the populations of levels 2 and 3 to be accurately known. Since none of the higher Balmer lines is observed to show emission, all are formed almost entirely in the photosphere. On the other hand, leading lines in the higher series, with their large *gf*-values, could well be formed in the wind. For example, Figure 7 shows the synthetic profile of  $P\alpha$  from model CYG 19; an emission spike rises out of the center of the photospheric Stark absorption line. Only a minor alteration in the structure of the model might change the synthetic feature from an emission line to an absorption line; absence of emission above the continuum in an observed profile should not be taken to mean that the basic structure of our models is unrealistic. By the same token, the morphology of this line could be a sensitive discriminant among models. Although this wavelength region is heavily obscured by telluric water vapor,

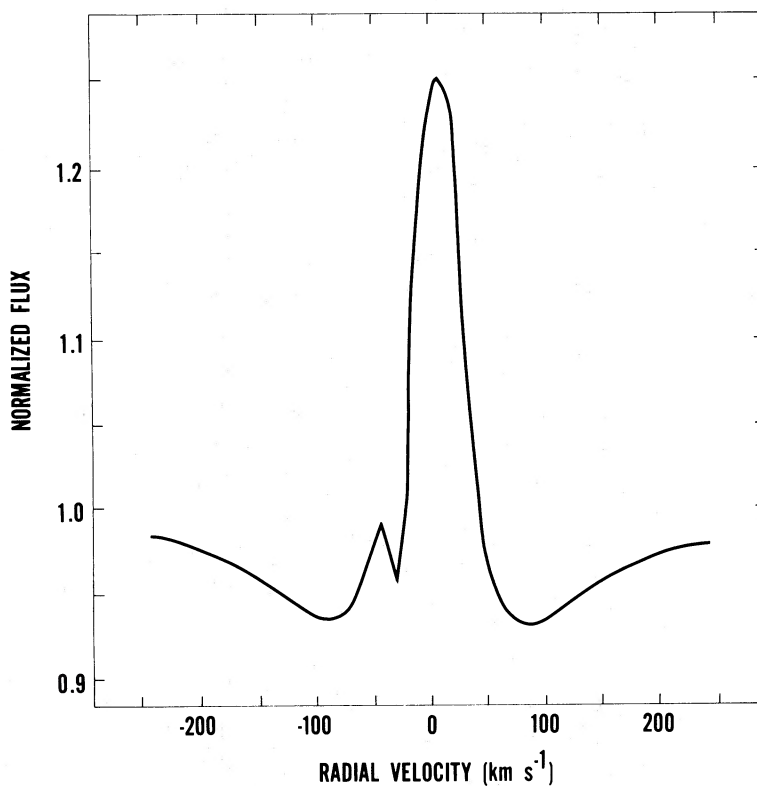


FIG. 7.—Paschen- $\alpha$  profile computed for model CYG 19

observations of Pa $\alpha$  are possible from very dry observatory sites, and would be of great interest for choosing the best model of the wind of  $\alpha$  Cyg.

#### VI. CONCLUSIONS AND DISCUSSION

Our comparison of synthetic H $\alpha$  profiles with the observed profiles in  $\alpha$  Cyg leads us to the following conclusions. First, a spherically symmetric, steady-state model, with the network of hydrogen transitions treated in detail, can fit the deeper observed profiles but not the shallower ones. Second, the models with the large microturbulent velocities that are required to fit the Mg II resonance-line profiles are also successful, although not required, here. Third, our modeling imposes constraints on the velocity law in the wind of a  $\alpha$  Cyg. Unless the model winds are fairly extended (large  $\beta$ ), the computed absorption minima are too deep, with radial velocities that are too negative. The softest velocity profiles (largest values of  $\beta$ ) are indicated for the narrowest absorption profiles among those presented by Inoue (1979).

Finally, our results indicate that, within the context of the turbulent models and the set of parameters used therein, the mass loss rate of  $\alpha$  Cyg is  $(1.7 \pm 0.4) \times 10^{-7} M_{\odot} \text{ yr}^{-1}$ . The range of values of  $\dot{M}$  that we obtain for various other values of the parameters suggests that a good estimate for the overall uncertainty of our determination is about a factor of 2. Our mass loss rate is consistent with the conclusion of Inoue and Uesugi (1977), from an analysis of shortward-shifted, strong lines of singly ionized metals, that the mass loss rate is  $1.0 \times 10^{-7} M_{\odot} \text{ yr}^{-1}$ .

It is interesting to compare our result with two other recently derived values of the mass loss rate of this star. From an analysis of shortward-shifted absorption components of low-excitation Fe II lines, Hensberge *et al.* (1982) derived an upper limit of  $5 \times 10^{-9} M_{\odot} \text{ yr}^{-1}$ . In order to minimize the dependence of their result on the ionization fraction, they used the absence of a shortward-shifted component in the Al III resonance lines to set a good lower limit on the population of Fe<sup>+</sup>. They included a detailed treatment of blending with neighboring photospheric lines, and, although they used the Sobolev approximation, their analysis appears sound. Nevertheless, a mass loss rate on this order yields no filling-in whatsoever of the H $\alpha$  line, according to several different lines of reasoning. First, the line optical depth in H $\alpha$  along any ray, as calculated in the Sobolev approximation (see Mihalas 1978, p. 479), is much smaller than unity if  $\dot{M} \sim 10^{-9} M_{\odot} \text{ yr}^{-1}$ . Second, a calculation of an emergent H $\alpha$  profile in which LTE was used as a first approximation to the populations of levels 2 and 3 of hydrogen, and in which  $\dot{M} \sim 10^{-9} M_{\odot} \text{ yr}^{-1}$ , gave a result hardly different from the photospheric profile. Third, the detailed analysis described here yields nearly the same result, as one would expect, since, in these models the departure coefficients of these levels are on the order of, though somewhat greater than, unity. We do not understand how this low mass loss rate could be correct.

On the basis of a nondetection of  $\alpha$  Cyg with the Very Large Array at a wavelength of 6 cm, Abbott (1980) places an upper limit of  $1.5 \times 10^{-7} M_{\odot} \text{ yr}^{-1}$  on the mass loss rate of  $\alpha$  Cyg. The value we have derived from nonturbulent models violates this limit only marginally. In order to compare Abbott's value with the value derived from our turbulent models, we need to take into account the fact that a mass loss rate derived from radio observations is proportional to the value assumed for  $v_{\infty}$ . If our turbulent models are correct, then the value of  $v_{\infty}$  to be used in deducing the mass loss rate should be divided by 2, and the upper limit on  $\dot{M}$  becomes  $8 \times 10^{-8} M_{\odot} \text{ yr}^{-1}$ . Then, our preferred value for  $\dot{M}$  exceeds the radio-inferred upper limit (unless  $R_{\text{ph}} \approx 80 R_{\odot}$ ).

In order to investigate whether this discrepancy is serious, consider the assumptions on which the derivation of a mass loss rate from a radio flux is based. The principal ones are that the wind is spherical, isothermal, and fully ionized (Wright and Barlow 1975; Panagia and Felli 1975). Of these, the third is the most apt to fail in our case. One result of the theory of free-free emission in an ionized wind is that the emission arises in the outermost layers. If these layers are predominantly neutral, then the nondetection at 6 cm would not be inconsistent even with mass loss rates much larger than we propose here.

We checked the possibility that the outer layers might be neutral by constructing a model envelope with outermost radius point at  $100R_{\text{ph}}$  (CYG 19). In the outermost shells of this model, hydrogen is indeed predominantly neutral, with a ground-state departure coefficient of  $8 \times 10^6$ . Since the wind is still very thick to Ly $\alpha$  at this distance, however, the truncating effect of a boundary there probably influences the results, and this check is not definitive.

As a further test, we ran a Sobolev calculation (which, of course, assumes zero Doppler width) for a six-level hydrogen atom, with the computer program used by Olson and Ebbets (1981). We generalized the program to evaluate the proton density self-consistently in the rate equations, which we restructured so that total number density,  $n(\text{H}) + n(\text{H}^+)$ , is conserved. The lower boundary condition for the solution of the equation of radiative transfer was taken from Kurucz's (1979) tables for  $T_{\text{eff}} = 9500 \text{ K}$  and  $\log g = 1.5$ . For a model that gave a reasonable fit to the observed profile, the result was predominant neutrality everywhere in the wind, with  $3 \leq n(\text{H})/n(\text{H}^+) \leq 15$ . Caution is advised here, since no one has closely examined the Sobolev calculation for applicability to winds cooler than 10,000 K. Nevertheless, these results indicate a possibility that the large volume outside the line formation zone of the subordinate lines may be neutral. Until this issue is better understood, mass loss rates should be inferred from radio data only for stars hotter than  $\alpha$  Cyg.

It is also interesting to compare our preferred mass loss rate with the run of values observed in O stars. If the luminosity of  $\alpha$  Cyg is  $2 \times 10^5 L_{\odot}$ , this star falls close to the mean relationship between  $\dot{M}$  and  $L$  given

by Garmany *et al.* (1981) for O stars in associations. This result tempts us to conclude that the mechanism driving the mass loss is the same for  $\alpha$  Cyg as for the hotter stars. If this mechanism is radiation pressure, then the number of driving lines required for this luminosity and for the mass loss rate we derive is about 30 (Lamers 1975; Kunasz and Praderie 1981). There is no doubt that this number of lines is present in the ultraviolet (Praderie, Talavera, and Lamers 1980).

If the same mechanism drives the wind in  $\alpha$  Cyg as in the hotter stars, one might expect the velocity laws to be similar. Therefore, we compare our conclusion that the narrow H $\alpha$  absorption profiles in  $\alpha$  Cyg require a value of  $\beta$  near 2 [i.e., a relatively slow increase of  $v(r)$  with  $r$ ] with recent results for hotter stars. On the theoretical side, Weber (1981) constructed a model for a radiation-driven wind and found  $\beta = 1$ . The semiempirical analysis of the Balmer lines in P Cygni by Kunasz and Van Blerkom (1978) indicates a slow velocity law. Both these results are consistent with ours.

What conclusion is to be drawn about the velocity laws in O and B stars in general is less clear. Olson and Ebbets's (1981) analysis of the H $\alpha$  emission line in 12 O and B giants and supergiants showed that a slow velocity law, with a gradient similar to that of our equation (3) for  $\beta = 2$ , is required by the observed profile in most cases. On the other hand, Abbott, Bohlin, and Savage (1982) analyzed the ratio of the emission equivalent width to the absorption equivalent width in the N v resonance-line profiles in 53 O and early B stars. By comparison with the prediction of a Sobolev calculation, they found that the smallness of this ratio requires  $\beta \leq 0.5$ ; larger values of  $\beta$  yield synthetic profiles in which the emission is too strong. The main-sequence stars generally demand the smallest values of  $\beta$ . The observations, however, may underestimate the amount of emission and overestimate the amount of absorption, because of weak blending absorption features. In addition, Hamann (1981) has shown that removing the Sobolev approximation would decrease the theoretical ratio for profiles in which the absorption is saturated. Thus, values of  $\beta$  in the range 1 to 2 may not be incompatible with the N v profiles. We conclude that our results for  $\alpha$  Cyg are consistent with the velocity laws that are indicated for at least the more luminous O and B stars.

Although we did not set out to interpret time-dependent characteristics of H $\alpha$ , our results suggest a

possible cause for the variations from profile to profile within class *b*. In Figure 5, the profiles synthesized from models CYG 2 and CYG 8 represent fairly well two of the kinds of profile in class *b*: the former a profile with no emission above the continuum and a fairly broad absorption component, and the latter a profile with substantial emission above the continuum and a narrower absorption component (although, in this case, the synthetic profile is too deep). Since the principal difference between these two synthetic profiles lies in the parameter  $\beta$  in the velocity law (eq. [2]), the variations among the profiles within class *b* may be due to changes in the structure of the star's envelope that are well modeled by changes in  $\beta$ , provided that our models are a valid representation of the structure of the envelope.

Our failure to represent the profiles in class *a*, however, suggests that our models do not include all the physical processes that operate in the envelope. Our search of parameter space has convinced us that no reasonable model in the class we have considered can solve this discrepancy. Rather, we suspect that an unknown mechanism with time-variable efficiency acts to fill in the bottom of the absorption component. Since the central intensity of H $\gamma$  and of some strong lines of ionized metals are also observed to be variable (§ II), this mechanism may be responsible for all three phenomena.

Of the assumptions underlying our models, one of the strongest and most likely to be violated is mass flux continuity, as the following argument shows. The characteristic time for the flow in the wind of  $\alpha$  Cyg can be estimated from the radius or the spherical envelope and a typical wind speed:  $t = R/v \sim 2 \times 10^{14} \text{ cm} / (10^7 \text{ cm s}^{-1}) = 2 \times 10^7 \text{ s}$ , which is about 200 days. Since the semiregular variations in radial velocity and the significant variations of nonsaturated features formed in the wind occur on a time scale of 10–14 days, mass flux continuity probably does not hold. If some reasonable model giving the function  $\rho(r)$  could be developed, it should be included in future work.

Major support for this work came from NSF grant AST 78-27620, and partial support from NASA grant NSG 5359, both to The University of Toledo. One of us (P. B. K.) thanks the National Center for Atmospheric Research for several hours of time on the Cray-1 computer, and G. Olson for use of his Sobolev computer code and for helpful discussions. We thank L. S. Anderson for comments on the manuscript.

#### REFERENCES

- Abbott, D. C. 1980, private communication.  
 Abbott, D. C., Biegging, J. H., Churchwell, E., and Cassinelli, J. P. 1980, *Ap. J.*, **238**, 196.  
 Abbott, D. C., Bohlin, R. C., and Savage, B. D. 1982, *Ap. J. Suppl.*, **48**, 369.  
 Barlow, M. J., and Cohen, M. 1977, *Ap. J.*, **213**, 737.  
 Bonneau, D., Koehlin, L., Oneto, J. L., and Vakili, F. 1981, *Astr. Ap.*, **103**, 28.  
 Brunish, W. M., and Truran, J. W. 1982, *Ap. J.*, **256**, 247.  
 Conti, P. S. 1978, *Ann. Rev. Astr. Ap.*, **16**, 371.  
 de Loore, C. 1980, *Space Sci. Rev.*, **26**, 113.  
 Garmany, C. D., Olson, G. L., Conti, P. S., and Van Steenberg, M. E. 1981, *Ap. J.*, **250**, 660.  
 Griem, H. R. 1964, *Plasma Spectroscopy* (New York: McGraw-Hill).  
 Hamann, W.-R. 1981, *Astr. Ap.*, **93**, 353.  
 Hensberge, H., Lamers, H. J. G. L. M., de Loore, C., and Bruhweiler, F. C. 1982, *Astr. Ap.*, **106**, 137.  
 Humphreys, R. M. 1978, *Ap. J. Suppl.*, **38**, 309.  
 ———. 1979, private communication.  
 Humphreys, R. M., and Davidson, K. 1979, *Ap. J.*, **232**, 409.  
 Inoue, M. O. 1979, *Pub. Astr. Soc. Japan*, **31**, 11.  
 Inoue, M. O., and Uesugi, A. 1977, *Pub. Astr. Soc. Japan*, **29**, 149.

- Kunasz, P. B., and Praderie, F. 1981, *Ap. J.*, **247**, 949.  
Kunasz, P. B., and Van Blerkom, D. 1978, *Ap. J.*, **224**, 193.  
Kurucz, R. L. 1979, *Ap. J. Suppl.*, **40**, 1.  
Lamers, H. J. G. L. M. 1975, *Phil. Trans. R. Soc. London A*, **279**, 445.  
———. 1981, *Ap. J.*, **245**, 593.  
Lucy, L. B. 1976, *Ap. J.*, **206**, 499.  
Mihalas, D. 1978, *Stellar Atmospheres* (2d ed.; San Francisco: Freeman).  
Mihalas, D., and Kunasz, P. B. 1978, *Ap. J.*, **219**, 635.  
Mihalas, D., Kunasz, P. B., and Hummer, D. 1975, *Ap. J.*, **202**, 465.  
Olson, G. L., and Ebbets, D. 1981, *Ap. J.*, **248**, 1021.  
Panagia, N., and Felli, M. 1975, *Astr. Ap.*, **39**, 1.  
Praderie, F. 1979, private communication.  
Praderie, F., Talavera, A., and Lamers, H. J. G. L. M. 1980, *Astr. Ap.*, **86**, 271.  
Rosendhal, J. D. 1972, *Ap. J.*, **178**, 707.  
Spresart, B. S., and Morrison, N. D. 1982, in preparation.  
Underhill, A. B. 1981, in *The Universe at Ultraviolet Wavelengths*, ed. R. D. Chapman (NASA Conference Publication 2171), p. 135.  
Vidal, C. R., Cooper, J., and Smith, E. W. 1973, *Ap. J. Suppl.*, **25**, 37.  
Weber, S. V. 1981, *Ap. J.*, **243**, 954.  
Wright, A. E., and Barlow, M. J. 1975, *M.N.R.A.S.*, **170**, 41.

PAUL B. KUNASZ: 315 Skylark Way, Boulder, CO 80303

NANCY D. MORRISON: Ritter Observatory, The University of Toledo, Toledo, OH 43606